

# ADVANCED FUNCTIONAL MATERIALS

## Supporting Information

for *Adv. Funct. Mater.*, DOI 10.1002/adfm.202310596

Post-Synthetic Silver Ion and Sulfurization Treatment for Enhanced Performance in  $\text{Sb}_2\text{Se}_3$   
Water Splitting Photocathodes

*Pardis Adams, Ramon Schnyder, Thomas Moehl, Jan Böhler, Angel Labordet Alvarez, Mirjana Dimitrievska, Keith McKenna, Wooseok Yang\* and S. David Tilley\**

## Supporting Information

**Post-Synthetic Silver Ion and Sulfurization Treatment for Enhanced Performance in Sb<sub>2</sub>Se<sub>3</sub> Water Splitting Photocathodes**

*Pardis Adams, Ramon Schnyder, Thomas Moehl, Angel Labordet Alvarez, Mirjana Dimitrievska, Keith McKenna, Wooseok Yang\* and S. David Tilley<sup>a\*</sup>*

Metal Solutions	Photovoltage (V vs. RHE)	Photocurrent (mA/cm <sup>2</sup> )	Fill Factor (%)
CaCl <sub>2</sub>	0.261 ±0.0303	-15.1 ±0.832	31.4
CoCl <sub>2</sub>	0.191 ±0.0474	-14.2 ±1.85	25.4
NiCl <sub>2</sub>	0.0733 ±0.0367	-5.47 ±2.01	14.5
CuCl <sub>2</sub>	0.286 ±0.0129	-15.1 ±1.10	23.5
ZnCl <sub>2</sub>	0.296 ±0.0133	-14.5 ±1.23	25.7
Ga(NO <sub>3</sub> ) <sub>3</sub>	0.261 ±0.00380	-14.8 ±1.22	30.9
AuCl <sub>3</sub>	-0.0400 ±0.00470	-0.526 ±0.0655	-
AgNO <sub>3</sub>	<b>0.322 ±0.0105</b>	<b>-18.9 ±1.57</b>	<b>42.2</b>
Untreated	0.177 ±0.0346	-14.4 ±0.751	21.0
AgNO <sub>3</sub> + S	<b>0.390 ±0.00724</b>	<b>-18.0 ±1.42</b>	<b>28.6</b>

Table S1 – Screening of various simple metallic solution treatments at the interface of Sb<sub>2</sub>Se<sub>3</sub> and TiO<sub>2</sub>. Photovoltage, photocurrent at 0 vs. RHE, fill factor, and their respective standard deviations were measured and calculated.

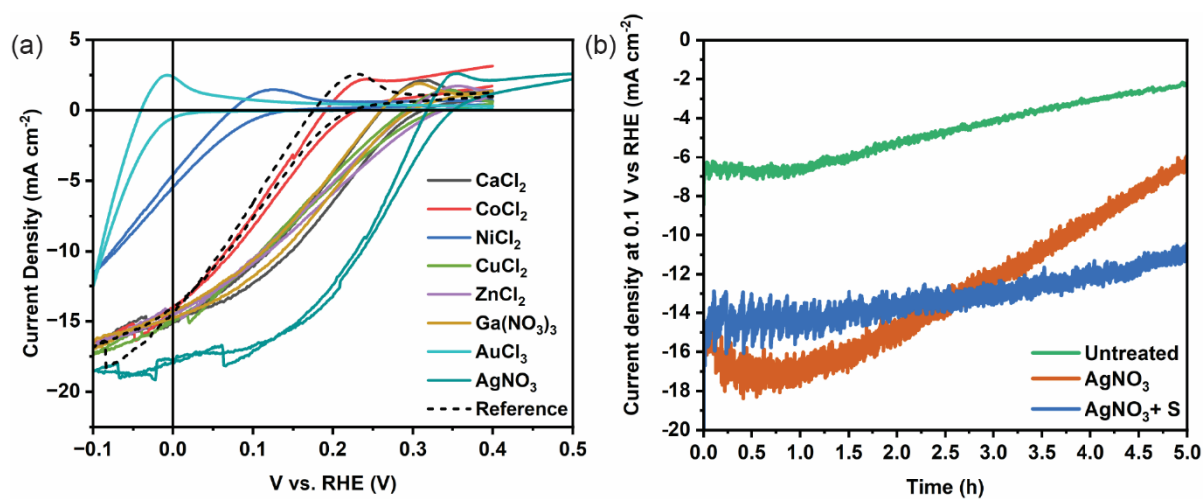


Figure S1 – (a) Cyclic voltammetry measurements of the metal screening experiment (b) Current density vs. time plots in 1 M H<sub>2</sub>SO<sub>4</sub> at 0 V vs. RHE at 1 sun illumination (100 mW cm<sup>-2</sup>) for 5 hours.

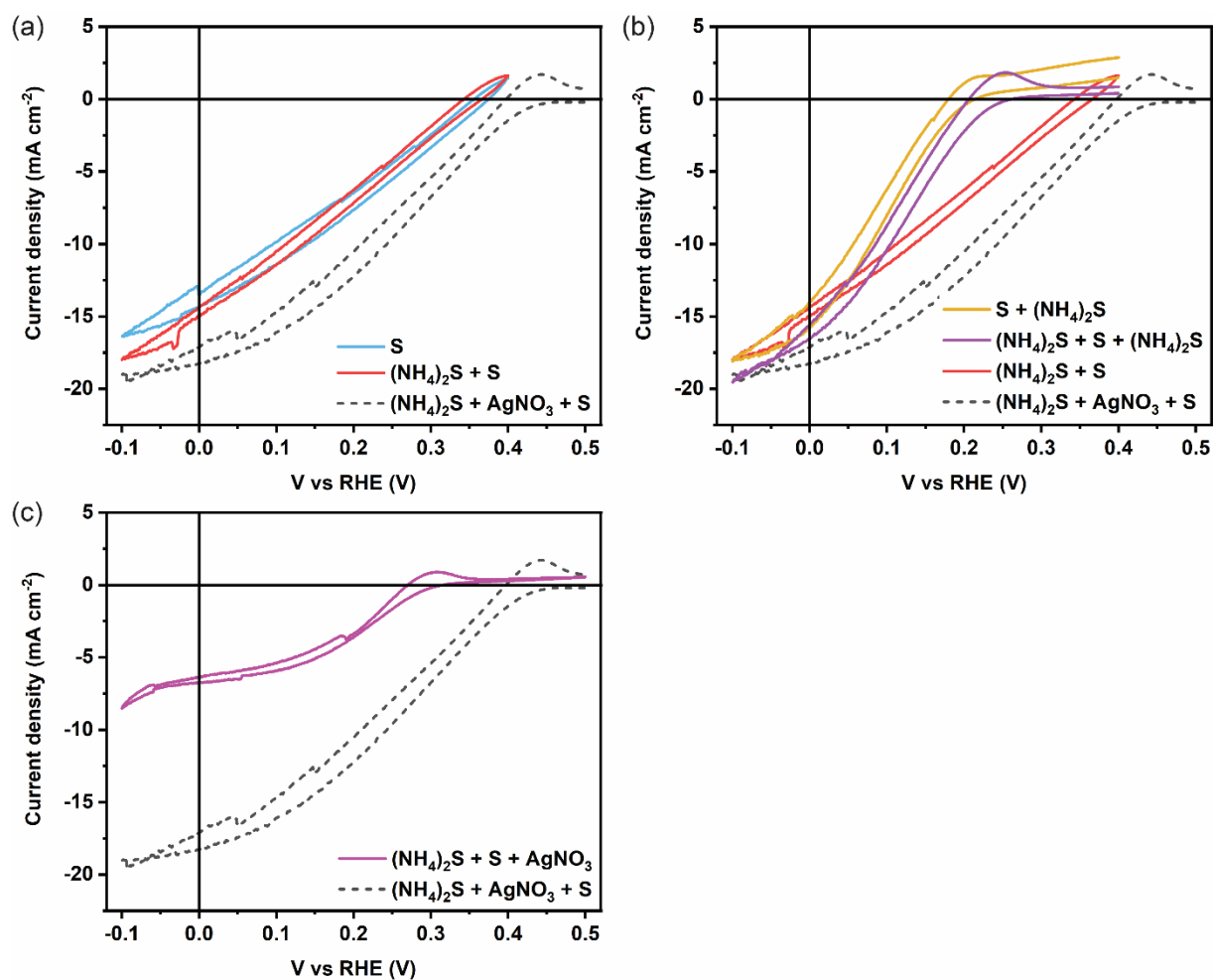


Figure S2 – All devices have a FTO/Ti/Au/Sb<sub>2</sub>Se<sub>3</sub>/TiO<sub>2</sub>/Pt configuration (a) only sulfurization treatment (blue) and (NH<sub>4</sub>)<sub>2</sub>S + sulfurization treatment (red) compared to the combined (NH<sub>4</sub>)<sub>2</sub>S + AgNO<sub>3</sub> + sulfurization treatment (b) (NH<sub>4</sub>)<sub>2</sub>S before (red), after (yellow) and both before and after (purple) sulfurization treatments compared to the combined (NH<sub>4</sub>)<sub>2</sub>S + AgNO<sub>3</sub> + sulfurization (c) AgNO<sub>3</sub> treatment before and after sulfurizations.

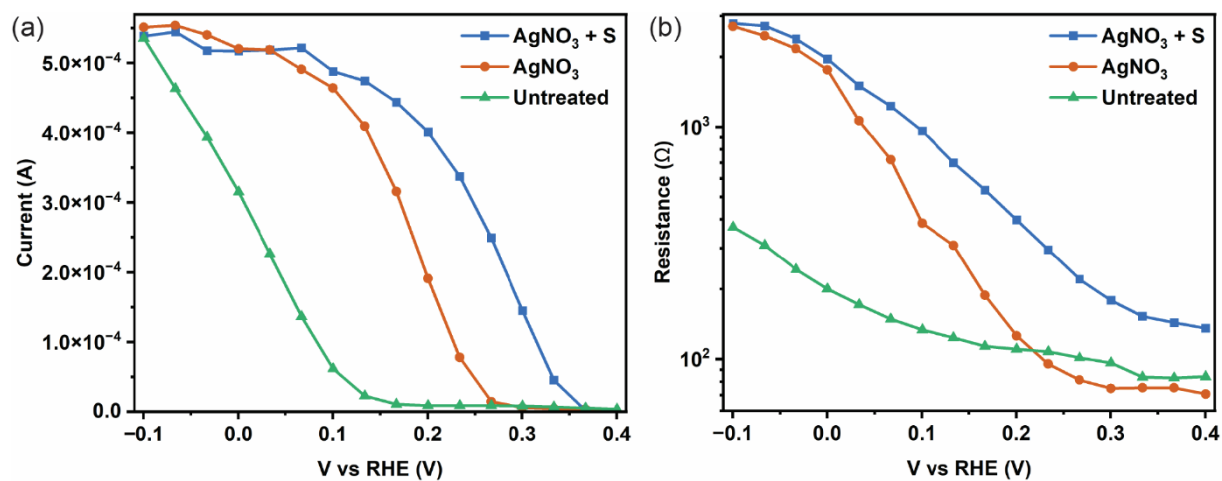


Figure S3 – All devices have a FTO/Ti/Au/Sb<sub>2</sub>Se<sub>3</sub>/TiO<sub>2</sub>/Pt configuration and were measured in 1M H<sub>2</sub>SO<sub>4</sub> at 10% white light from an LED light source (a) current vs voltage curves (b) resistance vs voltage determined from the EIS.

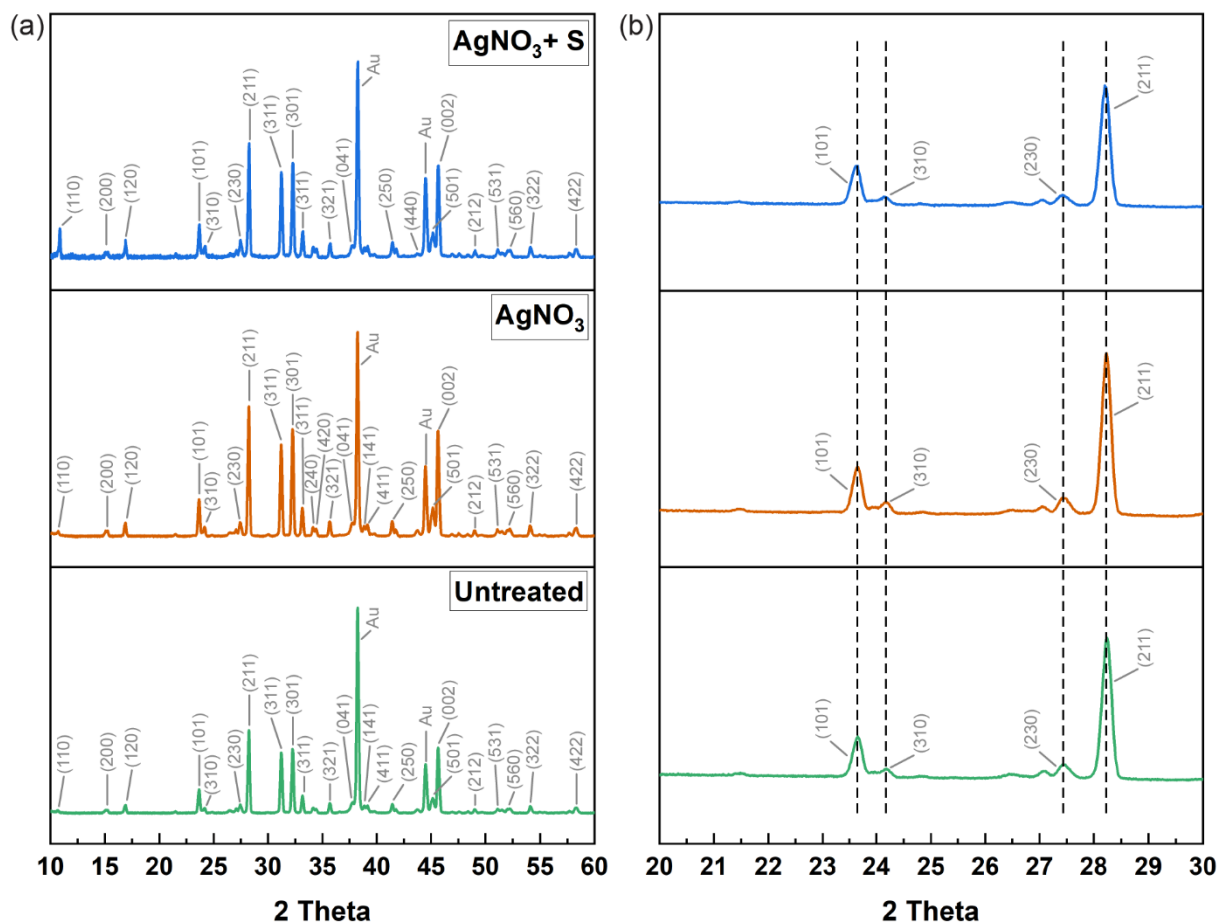


Figure S4 – (a) XRD patterns of untreated,  $\text{AgNO}_3$  treated, and  $\text{AgNO}_3$  + sulfurized treated  $\text{Sb}_2\text{Se}_3$  samples (b) Zoomed in view of the spectra to highlight lack of peak shifting.

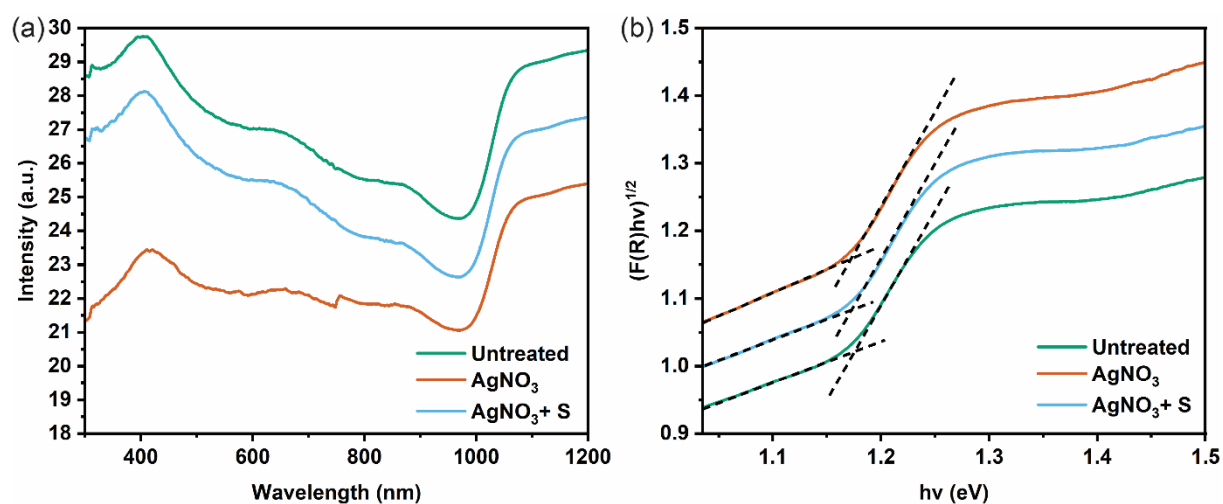


Figure S5 – (a) Diffuse reflectance spectra of the untreated, AgNO<sub>3</sub> and AgNO<sub>3</sub> + sulfurized Sb<sub>2</sub>Se<sub>3</sub> devices (b) A band gap of ~1.18 eV for all three samples was determined via the Kubelka-Munk (K-M) function.

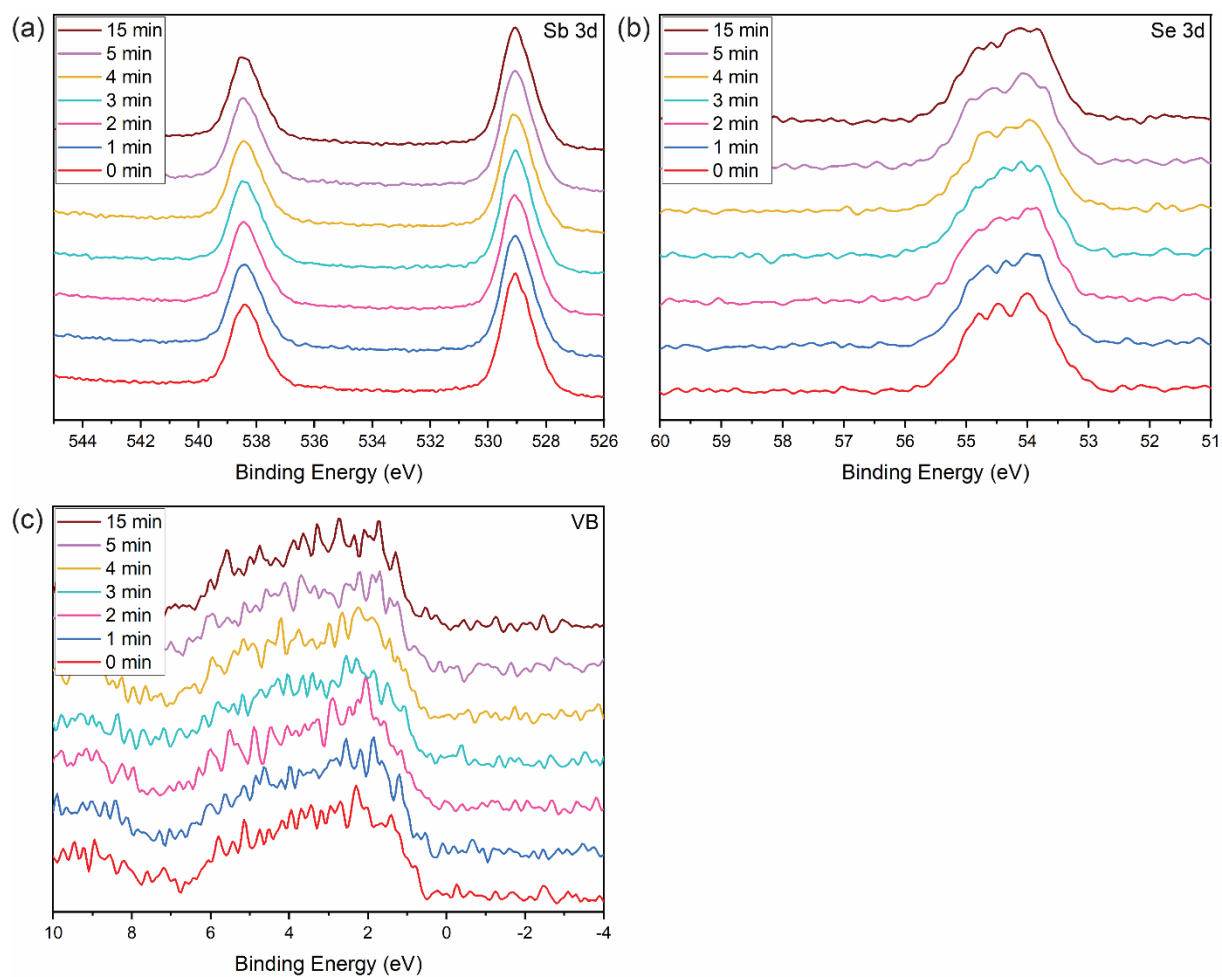


Figure S6 – XPS depth profiling of an untreated  $\text{Sb}_2\text{Se}_3$  sample sputtered at a  $\sim 35$  nm/min rate (a) Sb 3d core level (b) Se 3d core level, and (c) valence band maximum.



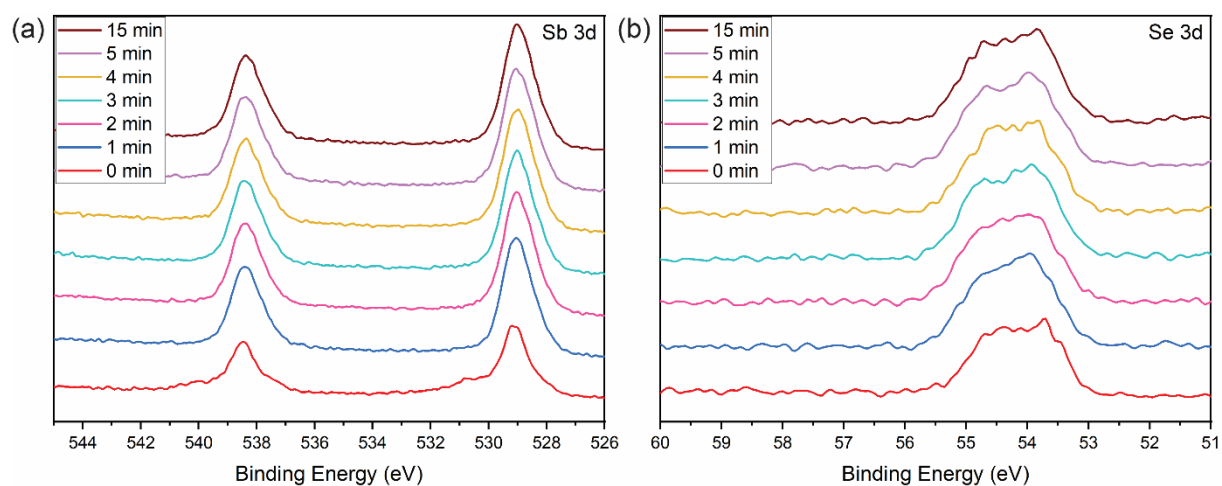


Figure S7 – XPS depth profiling of an  $\text{AgNO}_3$  treated  $\text{Sb}_2\text{Se}_3$  sample sputtered at a  $\sim 35$  nm/min rate (a) Sb 3d core level (b) Se 3d core level.

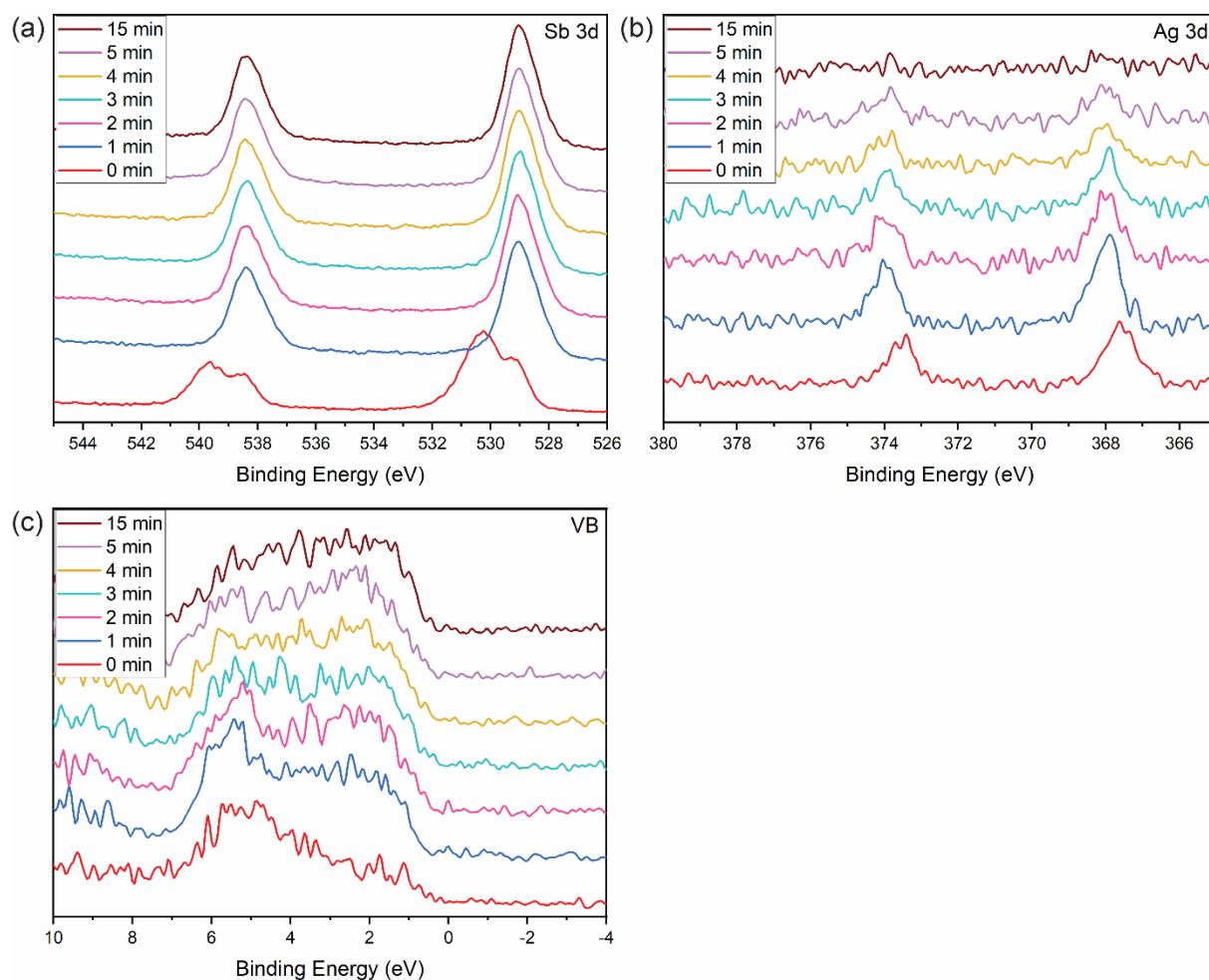


Figure S8 – XPS depth profiling of an  $\text{AgNO}_3$  + sulfurized  $\text{Sb}_2\text{Se}_3$  sample sputtered at a  $\sim 35$  nm/min rate (a) Sb 3d core level (b) Ag 3d core level, and (c) valence band maximum.

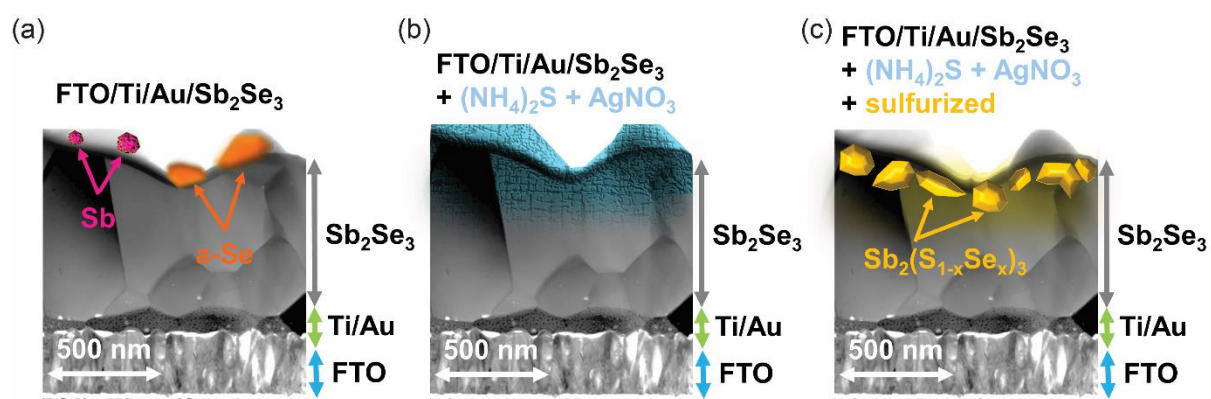


Figure S9 – Visual representation of each  $\text{Sb}_2\text{Se}_3$  sample based on Raman measurements (a) Metallic Sb and amorphous Se in an untreated  $\text{Sb}_2\text{Se}_3$  sample (b) Removal of metallic Sb and amorphous Se and integration of Ag into the  $\text{Sb}_2\text{Se}_3$  film (c) Formation of  $\text{Sb}_2(\text{S}_{1-x}\text{Se}_x)_3$  on the surface of the  $\text{Sb}_2\text{Se}_3$  film.

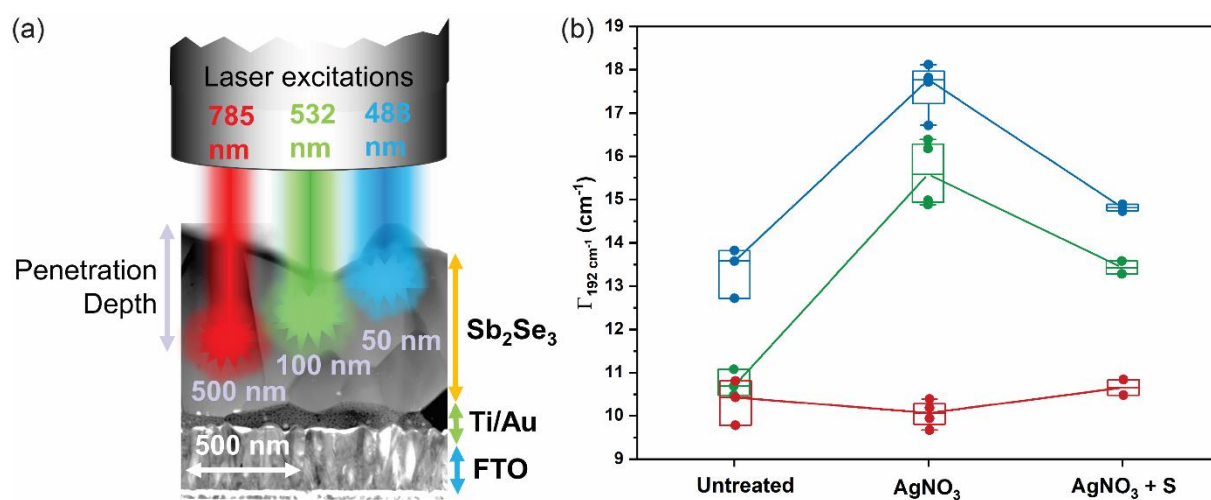


Figure S10 – (a) Visual representation of the penetration depth of the Raman lasers of each wavelength (b) Defect density and disorder levels of each sample when measured by the three different wavelengths of the Raman laser.

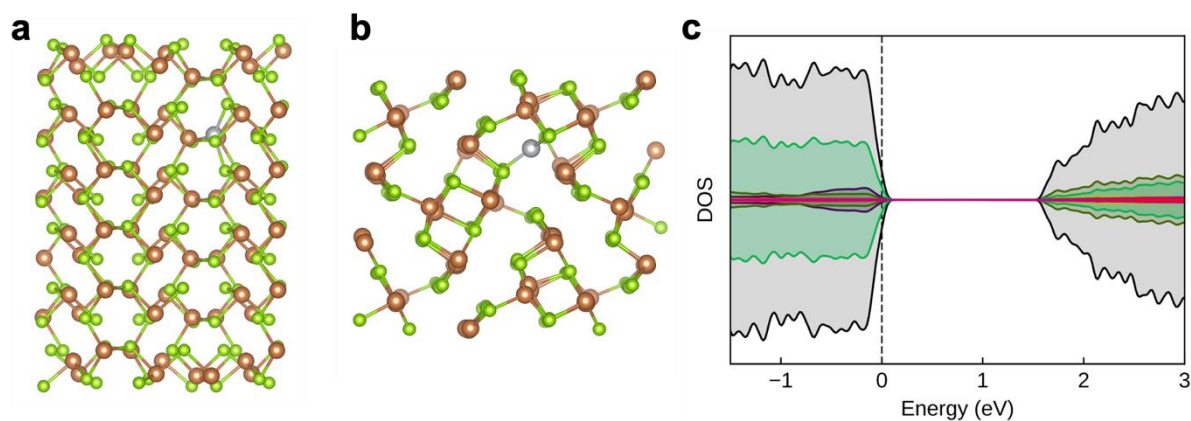


Figure S11 – (a) Side and (b) top views of the structure of the optimized structure of the  $\text{Sb}_2\text{Se}_3(001)$  surface with  $\text{Ag}^+$  incorporated between  $\text{Sb}_2\text{Se}_3$  ribbons below the surface. (c) The corresponding computed density of states showing no states are introduced within the band gap. Brown, green, silver, and yellow spheres represent Sb, Se, Ag, and S, respectively.